Nano World Journal

https://doi.org/10.17756/nwj.2024-s1-004

Research Article

Open Access

Modeling and Simulating the Effect of Car Brake Power Distributary on Carbon Nanofiber Brake Pads When Turning

Nguyen Thanh Tung* **and Luong Van Van**

Vinh Long University of Technology Education, Vinh Long City, Vietnam

***Correspondence to:**
Nguyen Thanh Tung
Vinh Long University of Technology Education, Vinh Long City, Vietnam.
E-mail: tungnt@vlute.edu.vn

Received: January 03, 2024
Accepted: March 04, 2024
Published: March 07, 2024

Citation: Tung NT, Van LV. 2024. Modeling and Simulating the Effect of Car Brake Power Distributary on Carbon Nanofiber Brake Pads When Turning. *NanoWorld J* 10(S1): S14-S18.

Copyright: © 2024 Tung and Van. This is an Open Access article distributed under the terms of the Creative Commons Attribution 4.0 International License (CCBY) (http://creativecommons.org/licenses/by/4.0/) which permits commercial use, including reproduction, adaptation, and distribution of the article provided the original author and source are credited.

Published by United Scientific Group

Abstract

The survey results about how the power of the brake distributary method on carbon nanofiber (CNF) brake pads affects an automobile's brake effectiveness are presented in this study. The authors constructed an automobile model of dynamics by decomposing the multi-body system's structure. Examining the impact of brake power distributary on carbon nanofiber brake pads on vehicle acceleration of the braking process using Matlab-Simulink software. The findings indicate that when a fully loaded driving Kia Pride vehicle is on a left roundabout with a radius of 100 m at a speed of 50 km/h. When driving a vehicle equipped with a brake power distributary system on CNF brake pads, there will be no tire locking, the back tires' brake power will rise by roughly 27%, and there will be a roughly 15% rise in the car's acceleration of the braking process. In case a car is without a brake power distributary method on CNF brake pads, the vehicle loses motion stability, and the back wheel locks and slips totally.

Keywords

Brake power, Distributary, Brake effectiveness, Carbon nanofiber brake pads

Introduction

Any braking system must have a brake pad, rotor, and caliper as its three main parts. By transferring kinetic energy into heat at the friction material and disc contact in the air, the friction material—that is, the portion of the brake pad that slides across the disc—plays a crucial role in slowing down and stopping a vehicle. The brake pad rolls against the disc when the caliper applies mechanical force to it during braking. During sliding, friction materials are exposed to enormous amounts of frictional heat generation, which causes wear on the rotor and the friction materials themselves as well as the development of particulate matter in different sizes [1]. One of the main causes, contributing as much as 21% of all particulate matter emissions associated with driving, is brake wear [2]. The size and chemical makeup of particulate matter particles, which are floating in the air, are constantly changing [3, 4]. Particle behavior in the human respiratory system varies due to the extraordinarily vast dimension range, which spans from a few nanometers to ten microns. Particles smaller than 10 μm may provide a threat to the terminal bronchioles, alveolar areas, and trachea-bronchial [5, 6].

Among the materials used to produce brake pads, carbon nanofiber materials are the most popular. Multi-walled carbon nanotubes (CNTs) are a class of materials that includes carbon nanofibers. CNFs are discontinuous, highly graphitic, and highly compatible with most polymer processing processes, and they can be disseminated in an isotropic or anisotropic mode. Thermoplastics, thermosets, elastomers, ceramics, and metals are just a few of the matrices that can benefit from CNFs' exceptional mechanical, electrical, and thermal conductivity.

Additionally, the special surface state of CNFs makes functionalization and other surface modification methods easier to apply, allowing the nanofiber to be engineered to fit the host polymer or application [7].

Unlike carbon fibers, which are continuous and have a diameter of several micrometers, CNFs are linear, noncontinuous filaments based on sp2. CNFs can be produced via electrically spinning polymerization of organic materials and heat treatment, as well as catalytic deposition by chemical vapor. Globally, about 500 tons of CNF are made available for purchase each year. Because of their nanosized diameter, CNFs have a high specific area, flexibility, and super strength. These characteristics make them appropriate for application as hybrid fillers in brake pads, tissue from bone scaffolds, and graphite fiber-reinforced polymeric materials. They are also utilized as electrode materials in energy storage devices. With their close relationship to carbon fibers and CNTs, CNFs are anticipated to become essential components of green science and technology [8].

The characteristics of the CNF are determined by its structure, which is influenced by the techniques employed during and after manufacturing. Typically, long, fibrous carbon layers that resemble platelets are piled one on top of the other in opposition to the direction to form fibers made of carbon. The catalyst that is used determines the configuration of the CNFs. To investigate the characteristics of the nanofibers, which have an average diameter of 50 - 200 nm and only one atom that is around 0.1 to 0.5 nm, sophisticated, cutting-edge microscopic techniques are needed.

They are small, but they have strong structural and chemical qualities. Following electrospinning, many polymers undergo heat treatment to preserve their excellent dimensional stability and electrical and thermal conductivities. They also offer good corrosion resistance and reinforcing characteristics, are relatively light, and are easy to form and process. Because there are fewer faults in CNF, its tensile strength rises as the fiber's diameter lowers. CNF tensile strength and fiber diameter fluctuate inversely, which means that as the fiber diameter decreases, so does how strong nanofibers of carbon are tensile. They have amazing flexibility. As the surface area/volume ratio increases, there is an increased area that is in contact with the filler and the matrix of polymers. The fibers are able to preserve their ratio without breaking or bending because of their increased flexibility. They also have a smoother, more elegant finish since the fillers are smaller [9].

CNFs have a 1.3 - 2 g/cm^3 of weight. Whereas the range of temperatures is 1950 to 6000 W/mK, the electrical resistivity is between 10^{-3} and 10^{-4}. For these materials, the ranges of tensile strength and tensile modules are 2.92 to 500 GPa and 240 to 1500 GPa, respectively. The CNF may be used as long as 100 nm and has 0.2 nm as the median pore radius. The CNF was subjected to sonication for either 20 sec at 120 W of output power or 6 min at 20 W. In every figure, the CNF's dimension ratio is 38. The axis of reference of the fiber determines the arrangement in which the nestled CNFs are arranged: either parallel or at an angle. As a result, the exterior of its frame has an enormous number of sensitive edges.

A high aspect ratio of strong adherence, homogeneous dispersion, and excellent dispersion between the CFRs and the polymer matrix are prerequisites for the presence of CNFs for producing multifunctional CFRs and polymer composites supplemented with remarkable mechanical characteristics. Melt mixing is the most widely used technique for creating composite compounds. Allowing CFRs to function, feeding CFRs after melting polymer pellets, using compatibilizers, and/or avoiding mixing conditions are additional crucial strategies to promote and facilitate CFR distribution and dispersion and to preserve the high CFR aspect ratio.

The mechanical properties of fibers made of carbon (CNTs) and polymer composites are not as good as those of CNTs and composites. One of the reasons is that CNTs have better inherent mechanical properties than CNFs. This clearly shows that producing CFRs with enhanced mechanical properties is necessary to produce multifunctional CFRs and polymer composites with lower filler loading. The melt spun polymer/CNFs composites have the best tensile strength properties reported thus far. To double the tensile strength and tensile modulus of composites formed by melt mixing and comparable techniques, ten percent of It was necessary to know the volume percent for CNFs. Since CFRs and polymer matrices are incompatible, functionalizing CNFs is a useful and essential technique to enhance the interface of both the polymeric matrix and the nanofiller. The methods for creating CNFs and polymers composites, melt spinning, *in-situ* polymers, coagulation, and grafted CNFs are not well documented. It is essential to look at the characteristics of CFRs and polymer composites created utilizing one of these processes in order to completely understand the reinforcing impact of CFRs and the ultimate attributes that their composites can exhibit. Fortunately, good investigations using CNTs have been completed; these studies can be used as a paradigm for additional study on CFRs in the future.

Compared to organic brake pads or metal brake pads, CNF brake pads have a higher price. In return, it has the best longevity and durability. Can withstand very high temperatures, has little wear and still provides good, responsive braking ability even when wet. Brake pads of this type of weigh only half as much as regular metal pads. Furthermore, they are not subject to corrosive effects from rainwater or salt in harsh conditions.

CNF material helps the brake mechanism function well even at high temperatures. In fact, they cause less wear on parts including brake pads and discs and also make less noise. The special structure helps absorb sounds and other noises to prevent them from entering the vehicle compartment. Helps eliminate noise completely and people in the car do not feel uncomfortable.

CNF brake pads are super durable and highly effective when used on vehicles. Helps make the car safer when traveling on the road, especially on the highway. These premium braking systems are 4 times more durable than conventional brakes. Ensuring long-term performance, resistance to harsh weather as well as dust and environmental pollution. The structure of the disc brake system and CNF brake pads is presented in figure 1 [10].

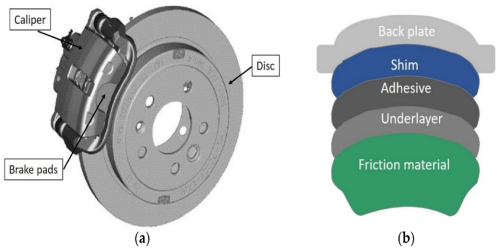

Figure 1: (a) Structure of a disc brake and **(b)** CNF brake pads [1, 10].

When a vehicle is driving on a roundabout, the power of inertia causes the load to be distributed on the tires to change. The way the tire grips the road determines the ideal bake power, that is, the optimal brake power depends on the tire load. The optimum brake power is determined in equation 1 [11].

$$P_{x\max} = P_z \mu_{x\max} \tag{1}$$

If $P_{x\max} = P_z \mu_{x\max}$ the braking process has not made full use of the grip of the tire, it will result in low brake effectiveness. In case $P_{x\max} = P_z \mu_{x\max}$ in addition to the tire being locked and slipping on the pavement, the brakes are not working as well. The car will have the best level of brake effectiveness if the brake power is applied in a way that maximizes tire grip. Either an electronic or mechanical brake power delivery system distributes the brake power applied to the vehicle.

Experimentation

The model of automobile dynamics

The technique of breaking down the multi-body system's structure to create an automobile model of dynamics was employed in the paper as shown in figure 2. The authors used Newton-Euler equations to construct an equation system for car dynamics as follows.

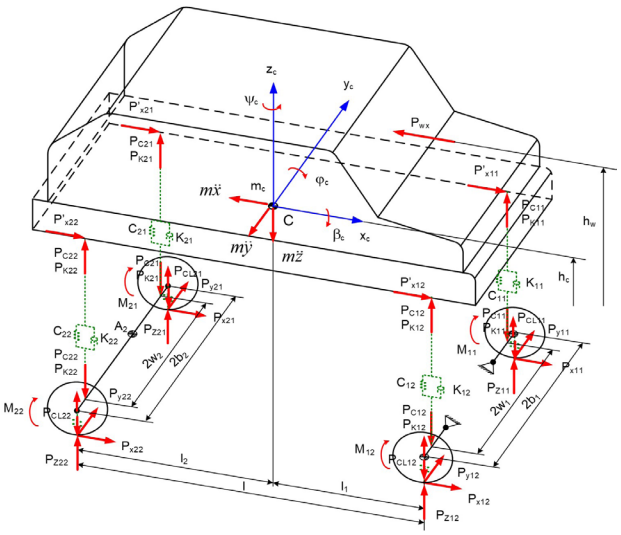

Figure 2: The automobile model of dynamics.

$$\left(m_c + m_{A11} + m_{A12} + m_{A2}\right)\ddot{x}_c = P_{x11}\cos\delta_{11} + P_{x12}\cos\delta_{12} - P_{y11}\sin\delta_{11} - P_{y12}\sin\delta_{12} + P_{x21} + P_{x22} \tag{2}$$

$$\left(m_c + m_{A11} + m_{A12} + m_{A2}\right)\ddot{y}_c = P_{x11}\sin\delta_{11} + P_{x12}\sin\delta_{12} - P_{y11}\cos\delta_{11} - P_{y12}\cos\delta_{12} + P_{y21} + P_{y22} \tag{3}$$

$$J_{zc}\ddot{\psi}_c = \left(P_{x11}\sin\delta_{11} + P_{x12}\sin\delta_{12} + P_{y11}\cos\delta_{11} + P_{y12}\cos\delta_{12}\right)l_1 + \left(P_{x22} - P_{x21}\right)w_2 + \left(P_{x12}\cos\delta 2 - P_{x11}\cos\delta_{11} + P_{y11}\sin\delta_{11} - P_{y12}\sin\delta_{12}\right)w_1 - \left(P_{y21} + P_{y22}\right)l_2 \tag{4}$$

$$m_c\ddot{z}_c = P_{C11} + P_{K11} + P_{C12} + P_{K12} \tag{5}$$

$$J_{yc}\ddot{\varphi}_c = \left(P_{C11} + P_{K11} + P_{C12} + P_{K12}\right)l_1 - \left(P_{C21} + P_{K21} + P_{C22} + P_{K22}\right)l_2 + M_{1j} + M_{2j} \tag{6}$$

$$J_{xc}\ddot{\beta}_c = \left(P_{C12} + P_{K12} - P_{C11} - P_{K11}\right)b_1 + \left(P_{C22} + P_{K22} - P_{C21} - P_{K21}\right)b_2 \tag{7}$$

$$m_{A12}\ddot{\xi}_{12} = P_{CL12} - P_{C12} - P_{K12} \tag{8}$$

$$m_{A12}\ddot{\xi}_{12} = P_{CL12} - P_{C12} - P_{K12} \tag{9}$$

$$m_{A2}\ddot{z}_{A2} = P_{CL21} + P_{CL22} - P_{C21} - P_{K21} - P_{C22} - P_{K22} \tag{10}$$

$$J_{Ax2}\ddot{\beta}_{A2} = \left(P_{C21} + P_{K21} - P_{C22} - P_{K22}\right)b_2 + \left(P_{CL22} + P_{KL22} - P_{CL21} - P_{KL21}\right)w_2 - P_{y21}\left(r_{21} + \xi_{A21}\right) - P_{y22}\left(r_{22} + \xi_{A22}\right) \tag{11}$$

$$J_{Ay11}\ddot{\varphi}_{11} = M_{A11} - M_{B11} - P_{x11}r_{d11} - P_{z11}e_{x11} = M_{A11} - M_{B11} - \left(P_{x11} - P_{z11}f_{11}\right)r_{d11} \tag{12}$$

$$J_{Ay12}\ddot{\varphi}_{12} = M_{A12} - M_{B12} - P_{x12}r_{d12} - P_{z12}e_{x12} = M_{A12} - M_{B12} - \left(P_{x12} - P_{z12}f_{12}\right)r_{d12} \tag{13}$$

$$J_{Ay21}\ddot{\varphi}_{21} = M_{A21} - M_{B21} - P_{x21}r_{d21} - P_{z21}e_{x21} = M_{A21} - M_{B21} - \left(P_{x21} - P_{z21}f_{21}\right)r_{d21} \tag{14}$$

$$J_{Ay22}\ddot{\varphi}_{22} = M_{A22} - M_{B22} - P_{x22}r_{d22} - P_{z22}e_{x22} = M_{A22} - M_{B22} - \left(P_{x22} - P_{z22}f_{22}\right)r_{d22} \tag{15}$$

Results and Discussion

The study examined the impact of brake power distributary on CNF brake pads on vehicle brake effectiveness using Matlab-Simulink software. Based on ISO 19747:2011 [12], the paper observed a Kia Pride driving around a roundabout with the condition that the car is fully loaded and turning left with a radius of R = 100 m (corresponding to the angle of rotation of the wheel is δ_i = 3° or the angle of the wheel of steering is δ_k = 54°), at the speed V_o = 50 km/h, the roadway where μ_{xmax} = 0.8 is the friction level; When surveying the braking torque applied brakes to the vehicle are $M_B = M_{Bmax} = P_G\mu_{xmax}r_d$; in this research, two automobile scenarios, one with and one without a brake power distributary system on carbon nanofiber brake pads, are examined; The survey time is 6 sec, with t = (0 ÷ 1)s is the time for the car to go straight, t = (1 ÷ 3) s is the time it takes the car to turn left with the turning radius R = 100 m, t = (3 ÷ 6)s is the braking time.

Figure 3 is a chart that displays the slide coefficient of the forward left tire S_{11} and the slip coefficient of the forward

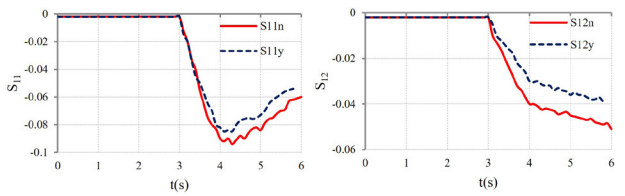

Figure 3: Coefficients of slippage of forward tires on both sides when turning left.

right tire S_{12}. The solid red line (S_{11n}) represents an unequipped vehicle with no brake power distributary on CNF brake pads; An automobile equipped with a brake power distributary system on CNF brake pads is shown by the blue dot line (S_{11y}). Based on the graph, it can be observed that the slip coefficient for the forward left tires in both the automobile with and without a brake power distributary system on CNF brake pads when braking has comparable forms and values, $S_{11n} \approx S_{11y} \approx$ 9%; In the two scenarios of the vehicle equipped with a brake power distributary system on CNF brake pads and the vehicle not equipped with one, the right forward tires have a value of $S_{12n} \approx S_{12y} \approx 5\%$.

The slip coefficient of the back tires can be seen in figure 4. If the vehicle has a brake power distributary system on CNF brake pads installed, the back tires' slip coefficient is $S_{21y} \approx S_{22y} \approx 6\%$, and the tires work stably within the area of elastic line. While the vehicle is not equipped with a brake power distributary system on CNF brake pads, the back tires' slip coefficient is $S_{21n} = S_{22n} = 100\%$, the tires fully slip and are locked, and the brake effectiveness of the car is reduced, and the car is destabilized.

The forward right and left tire's z-direction power is shown in figure 5. When the vehicle brakes, the forward tire's z-direction power increases. For the forward left tire's z-direction power: When t = (0 ÷ 1)s, the car moves on a straight road, $P_{Z11n} \approx P_{Z11y} \approx$ 2340N; When t = (1 ÷ 3)s, the car is moving around left, due to centrifugal power, there is less upward power on the forward left tire, $P_{Z11n} \approx P_{Z11y} \approx$ 1810N; When t = (3 ÷ 6)s, the car is both turning left and braking, due to the inertia and centrifugal power, the power in the

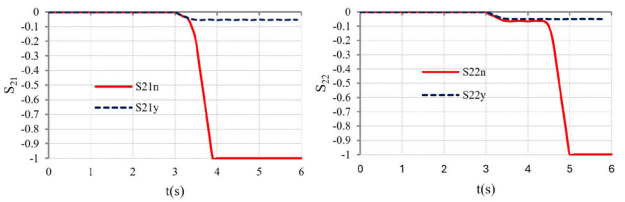

Figure 4: Coefficients of slippage of back tires on both sides when turning left.

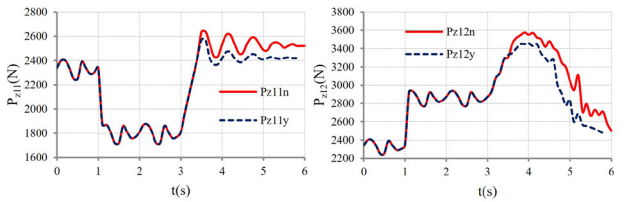

Figure 5: The forward right and left tire's z-direction power.

z-direction is more on the left in forward tire, the vehicle lacks a brake power distributary system on CNF brake pads $P_{Z11n} \approx$ 2500 N, brake power distributary system on CNF brake pads equipped vehicles has $P_{Z11y} \approx$ 2400 N.

For the forward right tire's z-direction power: When t = (0 ÷ 1)s, the car moves on a straight road, $P_{Z12n} \approx P_{Z12y} \approx$ 2340 N; When t = (1 ÷ 3)s, the car is moving around left, due to centrifugal power, the forward right tire's z-direction power is enhanced, $P_{Z12n} \approx P_{Z12y} \approx$ 2870 N; When t = (3 ÷ 6)s, the car is both turnings left and braking, due to the inertia and centrifugal power, the forward right tire's z-direction power is raised, the vehicle lacks a brake power distributary system on CNF brake pads has $P_{Z12n} \approx$ 3600 N, the brake power distributary system on CNF brake pads equipped vehicle has $P_{Z12y} \approx$ 3400 N.

Similarly, figure 6 is a chart of the z-direction power on the right and left back tires. For the z-direction power of the left back tire: When t = (0 ÷ 1)s, the car moves on a straight road, $P_{Z21n} \approx P_{Z21y} \approx$ 4010 N; When t = (1 ÷ 3)s, the car is moving around left, due to centrifugal power, the z-direction power on the left back tire is reduced, $P_{Z21n} \approx P_{Z21y} \approx$ 3450 N; When t = (3 ÷ 6)s, the car is both turnings left and braking, due to the inertia and centrifugal power, the z-direction power on the left back tire is further reduced, the car has no brake power distributary system and has $P_{Z21n} \approx$ 2600 N, the car with brake power distributary system on CNF brake pads has $P_{Z21y} \approx$ 2700 N.

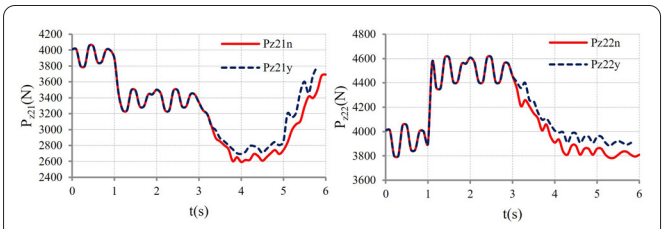

Figure 6: The back right side and left side tire's z-direction power.

For the z-direction power of the right back tire: When t = (0 ÷ 1)s, the car moves on a straight road, $P_{Z22n} \approx P_{Z22y} \approx$ 4010 N; When t = (1 ÷ 3)s, the car is moving around left, due to centrifugal power, the z-direction power on the right forward tire is increased, $P_{Z22n} \approx P_{Z22y} \approx$ 4500 N; When t = (3 ÷ 6)s, the car is both turnings left and braking, due to the inertia and centrifugal power, the z-direction power on the right forward tire is reduced, the car has no brake power distributary system on CNF brake pads has $P_{Z22n} \approx$ 3800 N, the car with brake power distributary system on CNF brake pads has $P_{Z22y} \approx$ 3900 N.

The longitudinal power of the right side and left side forward tires are shown in figure 7. The longitudinal power of the right side and left side forward tires in both of the situations of a vehicle using a brake power distributary system on CNF brake pads and a vehicle not one of the same size and shape, $P_{X11n} \approx$ 1700 N; $P_{X11y} \approx$ 1800 N; $P_{X12n} \approx P_{X12y} \approx$ 1850 N.

A graph showing the longitudinal power of the back tires on both the right and left sides is shown in figure 8. Whenever an automobile has a brake distributed power system on CNF

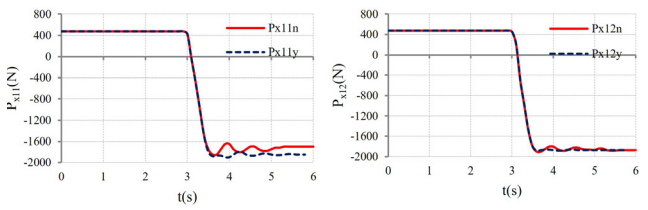

Figure 7: The forward right side and left side tire's longitudinal power.

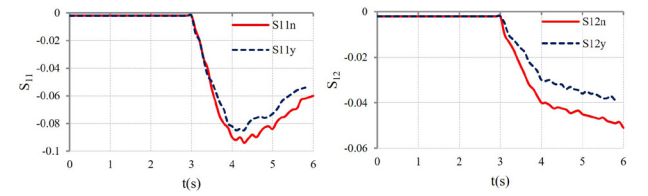

Figure 8: The longitudinal power of the back tires on the right and left sides.

brake pads, the longitudinal power of the back tires on the right side and left side is $P_{X21y} \approx P_{X22y} \approx 2600$ N. While an automobile has no brake power distributary system on CNF brake pads, the back tires have become locked and totally glide across the pavement, as a result, the longitudinal power of the right side and left side back tires is decreased, $P_{X21n} \approx P_{X22n} \approx 1900$ N. When an automobile is equipped with a brake power distributary system on CNF brake pads, its longitudinal power is approximately 27% higher than when it is not.

Figure 9 displays the car's acceleration of the braking process as well as the body rotation angle. When an automobile is equipped with a brake power distributary system on CNF brake pads, its acceleration of the braking process is around 15% bigger than when it is not. The acceleration of the braking process of an automobile is equipped with a brake power distributary system on CNF brake pads is $a_y = 7.0$ m/s^2, satisfying the ECE-R13 standard's requirements [13]. The acceleration of the braking process of an automobile does not have a brake power distributary system on CNF brake pads is $a_n = 6.0$ m/s^2. An automobile with a brake power distributary system on CNF brake pads has a body rotation angle of $\Psi_y \approx 6.0^\circ$, whereas an automobile without one has a body rotation angle of $\Psi_n \approx 7.5^\circ$.

Conclusion

Whenever a Kia Pride automobile is driven at 50 km/h on a left roundabout with a radius of R = 100 m and it is fully loaded, on the roadway where $\mu_{xmax} = 0.8$ is the friction factor. While an automobile has a brake power distributary system on CNF brake pads, the tires won't lock, the back tires' braking power will rise by roughly 27%, and the vehicle will accelerate the braking process by roughly 15%, all in accordance with the ECE-R13 standard [10]. The vehicle loses motion stability when the back wheel locks and slips fully in the absence of a braking power distribution system.

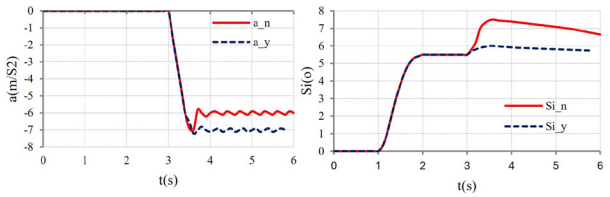

Figure 9: The acceleration of the braking process and the body rotation angle.

Acknowledgments

None.

Conflict of Interest

None.

References

1. Gautier di Confiengo G, Faga MG. 2022. Ecological transition in the field of brake pad manufacturing: an overview of the potential green constituents. *Sustainability* 14(5): 2508. https://doi.org/10.3390/su14052508
2. Grigoratos T, Martini G. 2015. Brake wear particle emissions: a review. *Environ Sci Pollut Res* 22: 2491-2504. https://doi.org/10.1007/s11356-014-3696-8
3. El-Fadel M, Massoud M. 2000. Particulate matter in urban areas: health-based economic assessment. *Sci Total Environ* 257(2-3): 133-146. https://doi.org/10.1016/S0048-9697(00)00503-9
4. Cambra-López M, Aarnink AJ, Zhao Y, Calvet S, Torres AG. 2010. Airborne particulate matter from livestock production systems: a review of an air pollution problem. *Environ Pollut* 158(1): 1-17. https://doi.org/10.1016/j.envpol.2009.07.011
5. Kastury F, Smith E, Juhasz AL. 2017. A critical review of approaches and limitations of inhalation bioavailability and bioaccessibility of metal(loid)s from ambient particulate matter or dust. *Sci Total Environ* 574: 1054-1074. https://doi.org/10.1016/j.scitotenv.2016.09.056
6. Kelly FJ, Fussell JC. 2012. Size, source and chemical composition as determinants of toxicity attributable to ambient particulate matter. *Atmos Environ* 60: 504-526. https://doi.org/10.1016/j.atmosenv.2012.06.039
7. Carbon Nanofiber Applications & Properties. [https://www.sigmaaldrich.com/IN/en/technical-documents/technical-article/materials-science-and-engineering/batteries-supercapacitors-and-fuel-cells/carbon-nanofibers] [Accessed March 07, 2024]
8. Kim YA, Hayashi T, Endo M, Dresselhaus MS. 2013. Carbon Nanofibers. In Vajtai R (ed) Springer Handbook of Nanomaterials. Springer, Berlin, pp 233-262.
9. Carbon Nanofiber. [https://nanografi.com/blog/carbon-nanofiber-cnf/] [Accessed March 07, 2024]
10. Papinniemi A, Lai JC, Zhao J, Loader L. 2002. Brake squeal: a literature review. *Appl Acoust* 63(4): 391-400. https://doi.org/10.1016/S0003-682X(01)00043-3
11. Jazar RN. 2019. Advanced Vehicle Dynamics. Springer.
12. ISO 14794:2011. Heavy Commercial Vehicles and Buses. Braking in a Turn. Open-loop Test Methods. [https://www.iso.org/standard/57256.html] [Accessed March 07, 2024]
13. Regulation No 13 of the Economic Commission for Europe of the United Nations. [https://op.europa.eu/en/publication-detail/-/publication/0a43f880-d612-11e5-a4b5-01aa75ed71a1/language-en] [Accessed March 07, 2024]